Potential-Dependent Electron Injection in Nanoporous Colloidal ZnO Films

P. Hoyer[†] and H. Weller*[,‡]

Hahn-Meitner-Institut, Kleinteilchenforschung Glienicker Strasse 100, D-14109 Berlin, Germany, and Institut für Physikalische Chemie, University of Hamburg, Bundesstrasse 45, D-20146 Hamburg, Germany

Received: March 28, 1995; In Final Form: June 13, 1995[⊗]

We have quantitatively investigated the charging of colloidal ZnO films by cyclic voltammetry and potential step measurements. Up to six electrons can be stored on each colloidal particle of the film (mean particle diameter 5.9 nm) before zinc reduction occurs. Fluorescence and absorbance of the films are already strongly influenced in potential regions where less than one electron is stored on each particle. Potentiostatically controlled and time-resolved photocurrent measurements show the influence of trap filling as well as the role of the electrolyte on the charge transport through the films.

1. Introduction

Small quantized semiconductor particles, which are currently being studied in many laboratories all over the world, exhibit a large potential for applications in the fields of electronics, optics, and catalysis.[1−6] Those applications mostly require an electric contact of the particles. It has been shown recently that the quantized electronic states of the particles are accessible by electrochemical means.[7−11] In these experiments, the optical and the electronic properties of the particles (e.g., absorption, fluorescence, and photocurrent) have been examined under potentiostatic control in solution as well as in the form of porous films consisting of aggregated particles. Most properties of the individual colloidal particles were retained also in the films, and the potential-dependent optical and electronic properties were found to differ significantly from those of the corresponding bulk materials. Consequently, the mechanisms of charge separation and the electron transport through nanoporous films are often discussed in a different way than it is done in the case of compact films or single crystals.[7,8,12,13]

In this paper, we will present cyclic voltammograms, electrically and optically detected potential step measurements, and potentiostatically controlled and time-resolved photocurrent profiles of colloidal nanoporous ZnO films. These experiments allow a quantitative measurement of the electron density of states. Moreover, we will discuss a dispersive electron-transport mechanism involving electrolyte-supported hopping processes.

2. Experimental Section

Zinc oxide films were prepared via a sol−gel process. The colloid was prepared by a method similar to that of Spanhel et al.:[14] 10.5 g of zinc acetate was refluxed with 500 mL of absolute ethanol. Two hundred milliliters of ethanol was allowed to evaporate within 3 h. A molar excess of 1.5 of LiOH × H_2O was added to the precursor in an ultrasonic bath to obtain a transparent solution of small quantized zinc oxide particles with diameters around 2 nm.

To 50 mL of the boiling zinc oxide solution, small amounts of water were added. During this procedure, the colloidal zinc oxide particles agglomerated and precipitated. The zinc oxide was separated from the supernatant solution by centrifuging and was washed twice with absolute ethanol. Finally, small amounts of absolute ethanol were added to the precipitate in order to obtain a viscous suspension of small zinc oxide particles. This suspension was used for spin coating (Convac Models 1001 and ST 146) on indium-doped tin oxide-coated glass (DESAG/Germany, sheet resistance lower than 30 Ω/sq). Film thicknesses of up to 4 μm were obtainable with good optical quality of the electrodes by repetitive coatings. The particle size distribution within the film has been carefully elaborated in ref 8. We have used electrodes from the same batch as in this reference and convinced ourselves that the particle size did not change between the respective measurements. A number-averaged mean diameter of 5.7 nm was derived from the histogram in this reference which corresponds to a volume-weighted mean diameter of 5.9 nm.

A pH 8 buffer (Merck, sodium borate/hydrochloric acid, 0.1 M) was used as the standard electrolyte. Ethanol (30 vol %) was added as a hole scavenger for the time-resolved photocurrent measurements and 0.1 M KI for the stationary ones, respectively.

The photoelectrochemical setup consisted of a Bank PGS 81 potentiostat or a Bank LB 75 L potentiostat combined with a Wenking VSG 83 scan generator. Steady-state illumination was performed with a 450-W high-pressure xenon lamp and a monochromator (Physics Instruments). The optical resolution was 20 nm and the light power was approximately 10 μW cm^{-2} at $\lambda = 360$ nm. The electrochemical cell consisted of a laser quartz cell (Radiant Dyes) equipped with the working electrode, an Ag/AgCl reference, and a platinum counter electrode.

Optical spectra were recorded with a Bruins Instruments Omega 20 spectrophotometer, and fluorescence measurements were performed with a Spex Fluoromax. Time-resolved optical absorbance changes of the film during a potential step were determined with the optical detection path of a flash photolysis apparatus which is described elsewhere.[15] Time-resolved photocurrent measurements were performed in the electrochemical cell after applying a 308-nm excimer laser flash (Lambda Physik, EMG 201 MSC, pulse duration 30 ns). Since the working electrode of the PGS 81 potentiostat is at ground level, the current at this electrode could easily be amplified by a home-made differential amplifier using a Fairchild microamp 733 video amplifier across a 100-Ω resistor. The time-resolved signals were sampled with a Tektronix TDS 620 oscilloscope and transferred to a personal computer. The baseline obtained with a closed shutter in the laser beam was subtracted from the

* To whom correspondence should be addressed.
[†] Hahn-Meitner-Institut.
[‡] University of Hamburg.
[⊗] Abstract published in *Advance ACS Abstracts,* August 1, 1995.

0022-3654/95/2099-14096$09.00/0

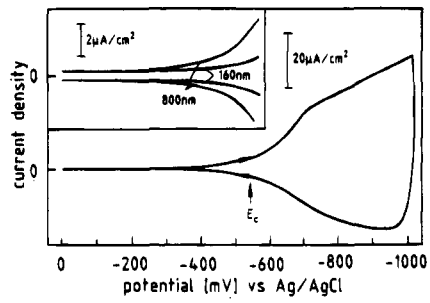

Figure 1. Cyclic voltammogram of a colloidal ZnO film in pH 8 buffer. Film thickness 1.3 μm, scan speed 10 mV s^{-1}. The inset shows cyclic voltammograms of colloidal ZnO films of 160- and 800-nm thickness, respectively. Scan speed as above. E_c indicates the "critical potential" of electron injection (see text).

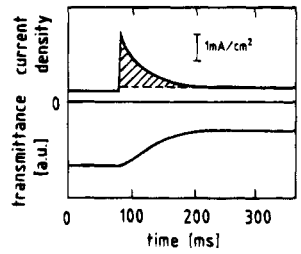

Figure 2. Upper: Current response after a potential jump from −600 to −900 mV. The capacitive load of the film was determined from the hatched area. Lower: Corresponding change of the optical transmittance of the film at λ = 360 nm.

signal. The time resolution of the setup was better than 1 μs, and the noise current determined with an uncoated ITO electrode was in the range of 10 nA.

Polarographic measurements were performed with a EG&G polarographic analyzer, Models 364 and 303 SMDE. The film thickness was measured with a Sloan Dectap 3030, and the size of the particles has been determined with a Philips CM 12 ST transmission electron microscope.

3. Results

Cyclic Voltammetry and Capacity Measurements. Figure 1 shows a cyclic voltammogram of a 1.3-μm-thick colloidal zinc oxide film in pH 8 buffer. Between 0 and −540 mV, only minor current response is observed, while at more negative potentials, the film becomes strongly charged. Reversing the scan direction results in a withdrawal of electrons from the film, i.e., a typical behavior for capacitive-like charging of the film. The process is not fully reversible and additional Faradaic processes like hydrogen evolution must be assumed between −600 and −1000 mV. The inset of Figure 1 shows the results obtained with films of different thicknesses on an enlarged scale. Between 0 and −250 mV vs Ag/AgCl, the current is independent of the film thickness. We, therefore, interpret this part of the cyclic voltammogram as capacitive charging of the ITO substrate which is in contact with the electrolyte through the nanoporous films. Negative from −250 mV, the measured currents increase with increasing film thickness, indicating the presence of vacant electron states in zinc oxide.

In order to measure the capacitive load of the electrodes more accurately, we have applied a potential step technique. Figure 2 shows the transient response of a 200-nm-thick colloidal ZnO film upon a potential step from −600 to −900 mV. The upper part of the diagram shows the time-resolved current response, while the corresponding optical transmittance changes near the band edge (λ = 360 nm) are depicted in the lower part of the figure. It is readily seen that the decay of the current after the potential jump follows the same kinetics as the optical bleaching,

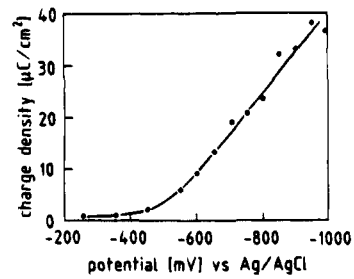

Figure 3. Charge density of a 0.7-μm-thick ZnO film as a function of the applied potential. The data were obtained from potential step measurements (see text).

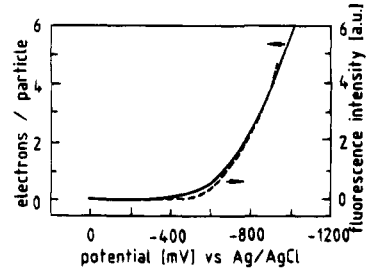

Figure 4. Number of deposited electrons per ZnO particle and intensity of the excitonic fluorescence as a function of the applied potential.

indicating that optical bleaching is caused by stored electrons as already proposed from radiolytic experiments.[16]

Potential step experiments were carried out in steps of 50 mV toward negative potentials between 0 and −1000 mV. In all cases, the potential jump induced current decayed in an exponential manner as expected for a simple *RC* term. The charges necessary for the respective potential steps were obtained by integrating the time-resolved current profiles as indicated in the upper part of Figure 2. The constant dc level after approximately 200 ms was attributed to Faradaic processes and was, therefore, neglected during integration. The results of the potential step measurements are shown in Figure 3. The values on the abscissa scale correspond to the end potential after the potential jump, e.g., the point at −600 mV gives the integrated charge after a potential jump from −550 to −600 mV. Whereas only minor charge contributions are recognized positive from −500 mV, the charges necessary for the potential jump linearly increase at more negative potentials, meaning that the capacity of the film steadily increases in this potential range.

Figure 4 shows the total charge of the film as a function of the applied potential, expressed as the number of electrons per ZnO particle, *n*, of the film. These values were obtained from the sum of the charges from Figure 3, *Q*, the mean volume-weighted particle diameter, $2r$ = 5.9 nm, and the total mass of zinc oxide, *m* (determined polarographically after dissolving the ZnO film in diluted hydrochloric acid),

$$n = \frac{4Q\pi r^3 \varrho}{3em}$$

ϱ = 5.6 g cm^{-3} is the density of bulk ZnO. It is readily seen from this formula that small deviations in *r* result in a relatively large error of *n*. However, the electron microscopically determined radii are accurate at least within 15%, leading to a maximum error for *n* of 50%. From Figure 4, it is recognized that positive from −500 mV, less than 1 electron is stored on each particle, while at increasingly negative potential, up to 6 electrons can be deposited (or 1 electron per roughly 700 ZnO molecules at −1 V). The number of electrons stored on each particle was found to be independent of the film thickness, indicating a constant morphology throughout the films.

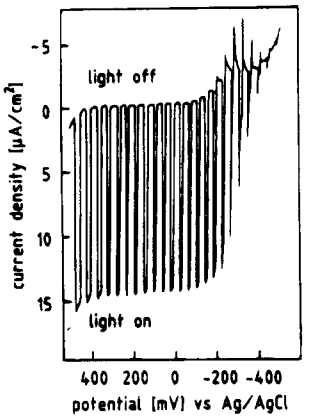

Figure 5. Linear sweep voltammogram taken under chopped illumination with light of $\lambda = 360$ nm: 0.1 M KI/pH 8 buffer, film thickness 1.3 μm, scan speed 10 mV s^{-1} toward negative potentials.

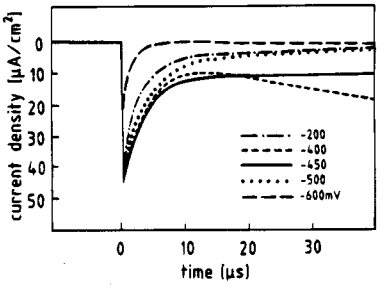

Figure 6. Time-resolved photocurrents (fast component) at various potentials measured after exposure to a 308-nm laser flash (30-ns pulse, pulse energy 5 μJ cm^{-2}, pH 8 buffer).

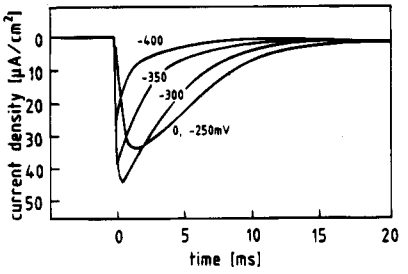

Figure 7. Time-resolved photocurrents (slow component, conditions as in Figure 6).

Also shown in Figure 4 is the increase of the excitonic fluorescence at $\lambda = 370$ nm under cathodic polarization, taken from ref 8 (dotted line). It is readily seen that the fluorescence intensity is directly proportional to the deposited charge.

Photocurrent Measurements. Stationary photocurrent measurements were performed in pH 8 buffer with 0.1 M KI as the hole scavenger. Maximum incident photon-to-current efficiencies of 30% were achieved independent from the film thickness under conditions of almost complete light absorption. In all cases, the onset of the photocurrent occurred at the onset of the optical absorption of the respective films. Figure 5 shows a linear sweep voltammogram under chopped illumination. Positive from −200 mV, the photocurrent and the dark current remain almost constant, whereas the photocurrent strongly decreases between −200 and −500 mV. Furthermore, the current observed immediately after opening the light shutter decreases within a few seconds of illumination by up to 40%, and an overshoot in the opposite direction is seen after switching the light off.

Figures 6 and 7 show the time-resolved photocurrent profiles after excitation with a 308-nm laser flash on different time scales and under various polarizations. Immediately after the laser pulse, a steep rise of the photocurrent is observed. This current decreases within 100 μs (we will call this the "fast component", Figure 6), and a slow component is built up and decays in the millisecond time regime (Figure 7). We have also measured decay curves using KI as a hole scavenger in order to prove that the decay profile is not interfered by a possible current-doubling process via electron injection by ethanol radicals. The shapes of the signals were very similar in both electrolytes except a baseline drift in the potential region between −200 and −400 mV in the case of KI, i.e., an effect which could already be observed in the stationary experiments (cf. Figure 5). The slow component represents most of the charge detected in the stationary experiments. At −250 mV, the maximum of the slow component is reached 2.5 ms after the excitation pulse. Whereas no changes in the kinetics of the slow component were observed positive from −250 mV, the rise and decay of the photocurrent is strongly accelerated at more negative potentials. Moreover, the total charge flow decreases with increasingly negative potentials. The shape of a charge vs potential plot obtained from the integrated slow component of the decay curves is very similar to the curve resulting from the stationary measurements. Similar changes in the decay kinetics with increasingly negative potential were also detected for the fast component (Figure 6). The decrease of the signal height, however, occurred at more negative potentials than in the case of the slow component. A detailed analysis of the charge passed through the electrode via the fast component is very difficult because of the uncertainty of the baseline level. One might be impinged to interpret the fast component as an artifact arising from the electrical circuit of the cell−amplifier−potentiostat-combination. We do not believe in this interpretation since the signal vanishes at negative potentials. Moreover, we superimposed a square pulse of a frequency generator at the connections of the electrochemical cell and observed the signal at the digitizer. No artifacts could be observed.

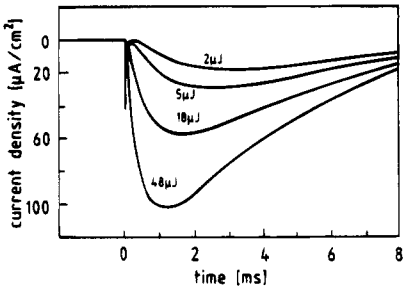

Figure 8. Time-resolved photocurrents (slow component) after excitation with various laser intensities.

The influence of the laser power on the photocurrent transients is depicted in Figure 8. The intensities of the fast and slow current components increase with increasing laser energy, and concomitantly, the maximum of the slow component is reached at shorter times after the laser pulse.

4. Discussion

In an earlier study,[8] we reported on the potential-dependent optical properties of ZnO samples which were identical to the ones described here. Three of the main results were as follows: (i) bleaching of the excitonic absorption band starts at a well-defined critical potential of $E_c = -540$ mV vs Ag/AgCl and increases with increasingly negative potential; (ii) excitonic fluorescence appears at E_c and rises with increasing cathodic polarization; (iii) E_c, which might be compared with the flat-band potential of bulk electrodes, directly scales with the quantization energy of the electrons within the individual particles of the film.

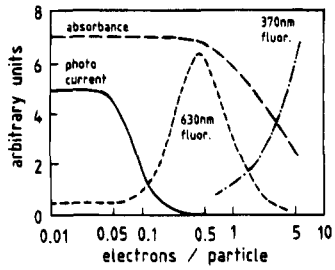

Figure 9. Photocurrent and absorbance, fluorescence intensities at 630 and 370 nm, respectively, as a function of the deposited charge per zinc oxide particle (see text).

In the cyclic voltammogram (Figure 1), E_c can be correlated with the steep rise of the reductive current. It is seen, however, that electron injection due to capacitive load of ZnO already starts around −250 mV, i.e., roughly 300 mV positive from E_c. The most obvious explanation arises from the size distribution of the ZnO particles. Since the particles are in the size quantization regime, the larger particles out of the distribution of sizes are expected to be reduced at more positive potentials, which would lead to a tail positive from E_c.[8,11] It was also shown in ref 8 that optical bleaching due to stored electrons is much less effective for larger particles than for smaller ones. This observation would explain why the onset of the optical bleaching with increasingly negative potential is much steeper than the onset of the reductive current. It is, however, easily estimated that fluctuations in the quantization energy of 5.9 ± 1.2-nm ZnO particles do not exceed 0.1 eV.[11,16] We, therefore, believe that the reductive tail in the cyclic voltammogram also reflects electron injection into vacant electron traps with trap depths of up to approximately 0.2 eV.

The potential step technique allows a quantitative measurement of the capacitive load of the ZnO film as demonstrated in Figures 2−4. It is noted that the differential capacitance obtained from Figure 3 is very large compared to plain metal electrodes of the same macroscopic size. This observation obviously results from the high internal surface area of the ZnO films.

The capacitance was found to linearly increase negatively from the critical potential, indicating a steadily increasing number of unoccupied electron states in the film. Thus, the position of the band edges should be rather stiff during charging of the particles, indicating an effective shielding of the excess charges by the surrounding electrolyte. We, therefore, do not believe that Fermi level pinning, i.e., a concomitant shift of the band edges with the Fermi level which should lead to a saturation of the electron injection, plays a significant role in the investigated potential region. It should be mentioned in this context that further charging of the films to more negative potentials than −1 V leads to an irreversible degradation of the electrodes due to zinc formation.

In ref 8, we have reported on the potential dependence of photocurrent, optical absorption, and fluorescence of colloidal ZnO films. With the results of the potential step measurements, we can express these properties as a function of the average number of stored electrons per particle, n. The respective plot is shown in Figure 9. The critical potential of $E_c = -540$ mV corresponds to a charge of roughly 0.5 electrons per particle. It is seen that only a relatively small number of electrons are required for strong optical bleaching. This finding is in agreement with radiolytic and photochemical investigations of ZnO colloids in solution.[16] Trapped fluorescence (at $\lambda = 630$ nm) is quenched by less than one electron. Similar behavior was also observed for ZnO colloids in solution.[17] In the case of the colloidal films, the interpretation is even more complicated since charge separation also competes with fluorescence.

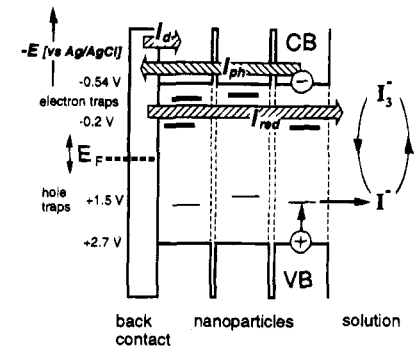

Figure 10. Energy scheme of the nanoporous ZnO electrodes and illustration of the electrochemical processes occurring under polarization and illumination. The shaded arrows give the direction of the electron flow of the capacitive dark current, I_d, the photocurrent, I_{ph}, and the reductive Faradaic current, I_{red}. The energetic position of the conduction band (CB) edge was taken from the critical potential, the valence band (VB) edge from the optical absorption. The trap depths for electrons were obtained from voltammetry and from the time-resolved photocurrent measurements. The mean trap depth for holes was estimated from the spectral position of the trapped fluorescence ($\lambda_{max} = 630$ nm).

Excitonic fluorescence (at $\lambda = 370$ nm) arises when one or more electrons are stored on a particle, whereby its intensity directly scales with the deposited charge (cf. Figure 4). We tentatively interpret this behavior by first blocking electron traps (at potentials positive from E_c) and by then an increase probability of recombination of free electrons with a photogenerated hole prior to its trapping.

Photocurrent. The linear sweep voltammogram of Figure 5 combines cyclic voltammetry with photocurrent measurements. The observed currents can be considered as the sum of the capacitive dark current due to charging of the film, I_d, a Faradaic current due to electrolyte reduction, I_{red}, and a photocurrent, I_{ph} (Figure 10, the arrows indicate the direction of the electron flow). Between +500 and −200 mV, I_d and I_{red} are practically zero and the anodic current observed under illumination directly gives the contribution of I_{ph}. The observed photocurrent efficiency of IPCE = 30% is considerably higher than the values reported by other authors.[10,18] We believe that these high values are due to an improved preparation procedure. Between −200 and −550 mV, vacant electron states of the film are gradually filled up, giving rise to a cathodic dark current, I_d. In this potential range, the anodic current under illumination decreases and so does the cathodic current during the dark periods. It is recognized that the differences of the currents observed immediately after opening and closing the light shutter during one illumination period, i.e., the contribution of I_{ph}, are almost equal. We, therefore, conclude that a reductive Faradaic process which depends on the illumination time strongly contributes to the shape of the voltammogram in this potential range. During illumination, I^- is oxidized, leading to the formation of I_3^- within the pores of the film. With increasing illumination time, I_3^- is enriched in the pores and can then be reduced electrochemically. Thus, with increasing illumination time, I_{red} should increase and the overall anodic current decreases. After closing the light shutter, I_{red} gradually decreases since the photogenerated I_3^- is consumed. As a net result, the cathodic current decreases until only the contribution of I_d is left.

The question arises why this type of behavior is not observed at more positive potentials since, thermodynamically, I_3^- could also be reduced in this potential range. I_3^- is formed within the pores close to the surface of the ZnO particles. Since the

diffusion of I_3^- to the ITO back contact is surely hindered by the morphology of the film, electrons have to be transferred through the ZnO film in order to result in an effective reductive current. At positive potentials, however, the ZnO film acts as an insulating layer, since no vacant electron states are accessible. Hence, I_{red} is directly coupled with I_d.

I_3^- reduction might also be expected to occur by the photogenerated electrons. Since, however, the photogenerated electrons are effectively transferred to the back contact, they only give rise to a very low stationary electron concentration in the film (see below), whereas the capacitive load of the film, I_d, results in a high stationary concentration of electrons (cf. Figure 4). Thus, the contribution of the photogenerated electrons to I_3^- reduction should be relatively small, which is reflected in the shape of the linear sweep voltammogram in the potential region between +500 and −200 mV. Here, the registered currents are almost constant during the illumination and dark periods, respectively.

Time-resolved photocurrents or photopotentials of porous titanium dioxide and zinc oxide films have been discussed in the literature by several authors.[18-20] In these measurements, either a two-electrode technique has been applied or the currents passed have been so large that the perturbations during the pulse did not allow a potential-dependent discussion. Distinct changes in the photocurrent transients were observed at potentials more negative than −250 mV, i.e., in the potential range where electron injection in the dark and drastic changes in the linear sweep voltammogram occur. Positive of −250 mV, the shape of the transients as well as the stationary photocurrents were almost constant. It is, therefore, obvious to explain the changes of the photocurrent kinetics as a result of trap filling, as was done in a similar way by Schwarzburg and Willig for microporous TiO_2 films.[20] Concerning this model, the transit time for electrons is determined by the release time out of the traps. In the case of our nanoparticulate films, this release time would correspond to an interparticle trap-hopping process, which might occur thermally activated and/or via tunneling. In any case, hopping should be as slow as the traps are deep. Thus, upon gradually filling the traps by increasing cathodic polarization, deep traps get more and more blocked for the photogenerated electrons and faster transport channels via shallow traps become increasingly active. In this sense, the photocurrent kinetics can be used as a highly sensitive monitor for vacant electron trap states in the films (cf. Figure 10).

Approaching the critical potential, the driving force for electron transport diminishes. Hence, we are faced with the situation that electron transport indeed becomes faster but less efficient, a behavior which is quite different to that of bulk electrodes.

The influence of trap filling on the photocurrent transients is also observed in the laser power dependence of the photocurrent profiles (cf. Figure 8). The maximum of the slow component is shifted to shorter times with increasing laser power, i.e., the first fraction of photogenerated electrons fills the deep traps and autocatalyses the transport of the following electrons.

The fast component of the photocurrent transients shows a far less pronounced potential dependence than the slow component (cf. Figures 6 and 7). The relatively fast transport and the breakdown of this component at more negative potentials than for the slow component suggest that the fast component arises from a small fraction of electrons which are also shallowly trapped under positive polarization.

The constant kinetics of the transients observed for the nanoporous ZnO electrodes positive from −250 mV indicates that field gradients play only a minor role during the electron transport. The electrochemical measurements, on the other hand, indicate that electron transport cannot be considered without taking into account the electrolyte within the pores between the interconnected particles. The ion clouds formed in the electrolyte around the trapped electrons prevent a net charging of the nanoporous electrode/electrolyte system in a spatially narrowly confined volume. Electron transport can be accompanied and favored by reorientation of the electrolyte, minimizing the occurrence of Coulomb blockades. In this sense, it becomes plausible that nanocrystalline semiconductor electrodes of TiO_2 and ZnO exhibit highly effective charge transport in electrochemical cells but are rather insulating in the form of solid-state devices with evaporated metal contacts.[21]

References and Notes

(1) Henglein, A. *Top. Curr. Chem.* **1988**, *143*, 113.
(2) Henglein, A. *Chem. Rev.* **1989**, *89*, 1861.
(3) Brus, L. E. *Appl. Phys. A* **1991**, *53*, 465.
(4) Wang, Y.; Herron, N. *J. Phys. Chem.* **1991**, *95*, 525.
(5) Weller, H. *Angew. Chem., Int. Ed. Engl.* **1993**, *32*, 41.
(6) Weller, H. *Adv. Mater.* **1993**, *5*, 88.
(7) Hodes, G.; Howell, I. D. J.; Peter, L. M. *J. Electrochem. Soc.* **1992**, *139*, 3136.
(8) Hoyer, P.; Eichberger, R.; Weller, H. *Ber. Bunsenges. Phys. Chem.* **1993**, *97*, 630.
(9) Kavan, L.; Stoto, T.; Grätzel, M.; Fitzmaurice, D.; Shklover, V. *J. Phys. Chem.* **1993**, *97*, 9493.
(10) Redmond, G.; O'Keeffe, A.; Burgess, C.; MacHale, C.; Fitzmaurice, D. *J. Phys. Chem.* **1993**, *97*, 11081.
(11) Hoyer, P.; Weller, H. *Chem. Phys. Lett.* **1994**, *221*, 379.
(12) Hagfeldt, A.; Björkstén, U.; Lindquist, S.-E. *Sol. Energy Mater.* **1992**, *27*, 293.
(13) Södergren, S.; Hagfeldt, A.; Olsson, J.; Linquist, S.-E. *J. Phys. Chem.* **1994**, *98*, 5552.
(14) Spanhel, L.; Anderson, M. A. *J. Am. Chem. Soc.* **1991**, *113*, 2826.
(15) Haase, M.; Weller, H.; Henglein, A. *J. Phys. Chem.* **1988**, *92*, 4706.
(16) Haase, M.; Weller, H.; Henglein, A. *J. Phys. Chem.* **1988**, *92*, 482.
(17) Bahnemann, D. W.; Kormann, C.; Hoffmann, M. R. *J. Phys. Chem.* **1987**, *91*, 3789.
(18) Hotchandani, S.; Kamat, P. V. *J. Electrochem. Soc.* **1992**, *139*, 1630.
(19) O'Regan, B.; Moser, J.; Anderson, M.; Grätzel, M. *J. Phys. Chem.* **1990**, *94*, 8720.
(20) Schwarzburg, K.; Willig, F. *Appl. Phys. Lett.* **1991**, *58*, 2520.
(21) Könenkamp, R.; Henninger, R.; Hoyer, P. *J. Phys. Chem.* **1993**, *97*, 7328.

JP950880H